JPET Fast Forward. Published on September 12, 2017 as DOI: 10.1124/jpet.117.242164
This article has not been copyedited and formatted. The final version may differ from this version.

Depletion of progranulin reduces GluN2B-containing NMDA receptor density, tau phosphorylation and dendritic arborization in mouse primary cortical neurons

Francesca Longhena, Michela Zaltieri, Jessica Grigoletto, Gaia Faustini, Luca La Via, Roberta Ghidoni, Luisa Benussi, Cristina Missale, PierFranco Spano and Arianna Bellucci[*].

Department of Molecular and Translational Medicine, University of Brescia, Brescia, Italy: FL, MZ, JG, GF, LL, CM, PS, AB

[2]*Molecular Markers Laboratory, IRCCS Istituto Centro San Giovanni di Dio Fatebenefratelli, Brescia, Italy: RG, LB*

Running Title: PGRN affects GluN2B-containing NMDA receptors

Address correspondence to:

Dr. Arianna Bellucci PhD,

Division of Pharmacology,

Dept. of Molecular and Translational Medicine,

University of Brescia,

Viale Europa no. 11

25123, Brescia, Italy

e-mail: arianna.bellucci@unibs.it

telephone: 0039 (0)30 3717380

fax: 0039 (0)30 3717529

Number of text pages: 40

Number of Tables: 1

Number of Figures: 6

Number of References: 62

Number of words in Abstract: 226

Number of words in Introduction: 851

Number of words in Discussion: 1304

JPET Fast Forward. Published on September 12, 2017 as DOI: 10.1124/jpet.117.242164
This article has not been copyedited and formatted. The final version may differ from this version.

Abbreviations

BSA: bovine serum albumin

DIV: days in vitro

EDTA: ethylenediaminetetraacetic acid

FTLD: Frontotemporal Lobar Degeneration

GAPDH: glyceraldehyde 3-phosphate dehydrogenase

GRN: granulin

KRS: Krebs Ringer solution

ICC: immunocytochemistry

IHC: Immunohistochemistry

LDH: lactate dehydrogenase

NGS: normal goat serum

NMD: non-sense mediated decay

NMDA: N-Methyl-d-aspartic-acid

PBS: phosphate buffered saline

PMSF: Phenylmethylsulfonyl fluoride

PRGN: progranulin

PVDF: Polyvinylidene difluoride

RNAi: RNA intereference

SCR: scramble

WB: western blot

JPET Fast Forward. Published on September 12, 2017 as DOI: 10.1124/jpet.117.242164
This article has not been copyedited and formatted. The final version may differ from this version.

Abstract

Loss-of-function mutations in the progranulin (PGRN) gene are a common cause of familial frontotemporal lobar degeneration (FTLD). This an age-related neurodegenerative disorder characterized by brain atrophy in the frontal and temporal lobes and with typical symptoms such as cognitive and memory impairment, profound behavioral abnormalities and personality changes, that are thought to be related to connectome dysfunctions. Recently, PGRN reduction has been found to induce a behavioural phenotype reminiscent of FTLD symptoms in mice by affecting neuron spine density and morphology, suggesting that the protein can influence neuronal structural plasticity. Here, we evaluated whether a partial haploinsufficiency-like PGRN depletion, achieved by using RNA interference in primary mouse cortical neurons, could modulate GluN2B-containing N-methyl-D-aspartate (NMDA) receptors and tau phosphorylation, that are crucially involved in the regulation of the structural plasticity of these cells. In addition, we studied the effect of PGRN decrease on neuronal cell arborization both in the presence and absence of GluN2B-containing NMDA receptor stimulation.We found that PGRN decline diminished GluN2B-containing NMDA receptor levels and density as well as NMDA-dependent tau phosphorylation. These alterations were accompanied by a marked drop of neuronal arborization, that was prevented by an acute GluN2B-containing NMDA receptor stimulation. Our findings support that PGRN decrease, resulting from pathogenic mutations, might compromise the trophism of cortical neurons by affecting GluN2B-contaning NMDA receptors. These mechanisms might be implicated in the pathogenesis of FTLD.

Introduction

Progranulin (PGRN), also known as granulin (GRN)-epithelin precursor, is a secreted pleiotrophic growth factor controlling the maintenance and regulation of the homeostatic dynamics of normal tissue development, proliferation, regeneration, immunity and inflammation (Jian et al., 2013; Petkau and Leavitt, 2014). Its role has been widely studied in the field of infectious diseases, wound healing, tumorigenesis, and most recently, neurodegenerative diseases. Indeed, GRN nonsense mutations, producing aberrant mRNA transcripts undergoing non-sense mediated decay (NMD), have been found to be responsible for the onset of familial forms of Frontotemporal Lobar Degeneration (FTLD) (Baker et al., 2006; Cruts et al., 2006; Skoglund et al., 2011; Gijselinck et al., 2008). All the pathogenic *GRN* mutations identified thus far cause the disease through a uniform mechanism, i.e. loss of functional progranulin or haploinsufficiency and FTLD results from progranulin depletion rather than from the accumulation of the mutant protein (Ghidoni et al., 2008; Ghidoni et al., 2012) (Finch et al., 2009; Sleegers et al., 2009). FTLD is a neurodegenerative disorder characterized by prominent atrophy of the frontal and temporal lobes of the brain and occurring in mid to later life. The typical symptoms encompass profound behavioral abnormalities, personality changes, progressive aphasia as well as other types of cognitive and memory impairment (McKhann et al., 2001).

In FTLD patients carrying a GRN mutation, the main pathologic signature on magnetic resonance imaging are the involvement of the fronto-temporo-parietal circuits, with prominent parietal and asymmetric atrophy (Bozzali et al., 2013; Rohrer et al., 2010; Whitwell et al., 2007), impaired connectivity in long-distance intrahemispheric tracts (Rohrer et al., 2013) salience network disruption (Borroni et al., 2012) and impaired brain oscillatory activity (Moretti et al., 2016).

Cortical atrophy and white matter tract abnormalities in frontal-parietal circuits can be detected at least a decade before the estimated onset of symptoms in asymptomatic mutation carriers (Pievani et

al., 2014; Rohrer et al., 2015) suggesting that connectome dysfunctions could be crucial for disease manifestation.

In the brain, PGRN is expressed in both microglial cells and neurons, but not in astrocytes. While GRN expression in neurons increases with cell maturation, its expression in microglia varies in relation to the activation state of the cells, and can be enhanced in response to excitotoxic injury (Petkau et al., 2010). Complete deficiency of PGRN has been found to dysregulate microglial activation, contribute to increased neuron loss with injury and promote circuit-specific synaptic pruning via complement activation (Lui et al., 2016; Martens et al., 2012). However, more recent studies reported differences in the effect of protein deficiency in multiple inbred mouse strains in relation to neuron spine density and morphology (Petkau et al., 2016), thus suggesting a complex role for PGRN in the regulation of neuronal resilience. Consistently, a biased lack of PGRN in mice can induce behavioural abnormalities that are reminiscent of FTLD symptoms such as age-dependent social and emotional deficits. These alterations occur in the absence of gliosis or increased expression of tumor necrosis factor-α, thus suggesting that FTD-related deficits can develop in the absence of detectable neuroinflammatory changes, and supporting an important effect of PGRN deficiency on neurons (Filiano et al., 2013). On the other hand, both full length PGRN and GRN-E peptide promote neuronal survival and neurite outgrowth in primary rat cortical and motor neurons (Ryan et al., 2009; Van Damme et al., 2008). PGRN has been also implicated in the regulation of motor neuron development as well as neurite outgrowth and branching (Chitramuthu et al., 2010; Laird et al., 2010) while gene silencing of PGRN in primary hippocampal neurons affects neuronal connectivity (Tapia et al., 2011). In line with these evidences, we demonstrated (Benussi et al., 2016) that the presence of GRN null mutations strongly reduces the number of released exosomes, microvesicles serving as intercellular communication tools that can be released by neurons following synaptic activation (Laulagnier et al., 2017).

Collectively, these evidences support that PGRN deficiency can affect neuronal structural plasticity.

Of note, this latter process can be finely regulated by the activity of glutamate N-Methyl-d-aspartic-acid (NMDA) receptors (Carpenter-Hyland and Chandler, 2007; Mony et al., 2009; Stein et al., 2015; Wyllie et al., 2013), and of those containing the GluN2B subunit in particular (El Gaamouch et al., 2012; Williams et al., 2003). GluN2B-containing NMDA receptors have been found to be implicated in the control of tau phosphorylation in cortical and hippocampal neurons (Arendt et al., 2015; Laurier-Laurin et al., 2014) and NMDA receptors can mediate tau-dependent neuronal degeneration (Tackenberg et al., 2013). Therefore, the resilience of cortical and hippocampal neurons, that are vulnerable in FTLD, may be particularly sensitive to subtle homeostatic changes in NMDA receptor function and tau post-translational modifications.

On this basis, we aimed at studying whether and how PGRN reduction could modulate the structural plasticity of primary cortical neurons by affecting the expression of NMDA receptors and tau phosphorylation. We found that PGRN gene silencing decreased GluN2B-containing NMDA receptor density and activity as well as NMDA-dependent tau phosphorylation without affecting cell viability. These events were accompanied by the onset of a marked reduction of the dendritic arborization of cortical neurons, that could be prevented by an acute stimulation of GluN2B-containing NMDA receptors.

Materials and Methods

Animals

C57BL/6J mice were used to prepare primary neuronal cell cultures and to characterize PGRN expression in the adult brain. Animals were bred and housed in the Animal House facility of the Department of Molecular and Translational Medicine of the University of Brescia with food and water and maintained on a 12-h light/dark cycle at a room temperature 23°C. All experiments and surgical procedures were conformed to the National Research Guide for the Care and Use of Laboratory Animals and were approved by the Animal Research Committees of the University of Brescia (Protocol Permit number 03/12 and 04/12). All efforts were made to minimize animal suffering and to reduce the number of animals used.

Primary cortical and hippocampal neuronal cultures

Primary neuronal cultures from cortical and hippocampal tissues were dissected from C57BL/6J newborn pups at day 0. Briefly, after mechanical dissociation the single cells were re-suspended in Neurobasal-A medium (Gibco, Milan, Italy) containing 100 µg/ml penicillin, 100 µg/ml streptomycin (Sigma-Aldrich, Milan, Italy), 0.5 mM glutamine (EuroClone, Milan, Italy) and 1% B27 supplement (Gibco). Cells were then centrifuged and cell count and viability assays were performed using the Trypan Blue exclusion test. Cells were seeded onto poly-D-lysine-coated glass coverslides in 24-well plates (14 µg/mL) for immunocytochemistry (70000 cells/well), or onto poly- D-lysine coated Petri dishes (10 µg/mL) for biochemical analyses (800000 cells/dish). Cells were maintained at 37°C under a humidified atmosphere of 5% CO_2 and 95% O_2 for at least 10 days in vitro (DIV) prior to their use to allow their maturation. Characterization experiments on cell cultures showed that they contained 95 % neuronal cells and 5 % astrocytes (results not shown).

JPET Fast Forward. Published on September 12, 2017 as DOI: 10.1124/jpet.117.242164
This article has not been copyedited and formatted. The final version may differ from this version.

RNA interference

Cortical neurons were subjected to RNA interference (RNAi) at DIV10 with four different siRNA sequences for PGRN gene silencing (Dharmacon, Chicago, USA). A non-silencing RNA sequence, scramble (SCR), was used as negative control. The optimal targeting and SCR RNA concentrations for gene silencing was estimated to be 25 nM.

All the sequences were diluted in Opti-MEM (Gibco) and then transfected into cells using INTERFERin (Polyplus-Transfection, Illkirch, France) according to the manufacturer' s instructions.

Lactate dehydrogenase (LDH) activity-based cytotoxicity assay

Cell culture media from either control primary neuronal cultures or cultures treated with siRNA or SCRwere centrifuged at 250g for 4 min to remove the cells debris. LDH activity measurements were performed using a commercially available assay (Sigma Aldrich, Italy) according to the manufacturer's instructions. The LDH activity was measured at 490 nm and 600 nm with a spectrophotometer.

Measurement of intracellular calcium concentrations

Regulation of cytosolic free Ca^{2+} concentration by NMDA in primary cortical neuronal cells was investigated by microfluorimetry in single cells according to Navarria et al., (2015). The cells were plated onto 50 ng/mL poly L-lysine-coated glass coverslips at a density of 0.5x 10^3 cells/cm^2 and cultured as described above. At DIV 10, cells were loaded with the Ca^{2+}-sensitive fuorescent dye Fura-2 AM (Sigma-Aldrich). Incubation was carried out for 60 min at 37 °C in Krebs Ringer solution (KRS) (125 mMNaCl, 5 mMKCl, 1.2 mM KH_2PO_4, 2 mM $CaCl_2$, 25 mM HEPES–NaOH, 6 mM glucose, pH 7.4) containing 1.3 mg/mL bovine serum albumin (BSA) and 4 mM Fura-2 AM. Then they were mounted in a 22-mm holder creating a chamber with the coverslips on the bottom. Fura-2 emission was monitored by using an inverted fluorescence microscope (Nikon Diaphot) associated

with an intensified charge-coupled device camera (MIRA-100 TE; Applied Imaging, Gateshead, UK) which recorded the 510 nm fluorescence emission in neurons excited through narrow band-pass filters (340 nm and 380 nm). The background was subtracted and the amount of free Ca^{2+} within the cell bodies was calculated from the ratio of 340/380 nm obtained every 3±4 s. Calibration was made according to external standards of Ca^{2+} and Fura-2. Fluorescent image acquisition and analysis were performed using the MIRACAL (Multiple Image Ratioing and Analysis with calibration system, by Applied Imaging, UK). Cells were exposed to 500 μM NMDA and 100 μM glycine for 200 sec in the chamber containing Mg^{2+}-free KRS. To check whether Ca^{2+} release was dependent on GluN2B-containing NMDA receptors cells were exposed to 1μM ifenprodil, which was added 30 s before glutamate and glycine stimulation and maintained for the entire experiment. Cells were then washed with Ca^{2+}-free solution and returned to the KRS. To check whether analyzed cells were sensitive to depolarizing stimuli, at the end of each experiment, 100 mM KCl stimulation was performed. Plateau values of $[Ca^{2+}]$ increase were calculated from the mean of four determinations taken at 20, 40, 60, 80 and 120 s after application of stimulating agents.

Cell culture treatments

To evaluate the effect of NMDA receptor stimulation on neuronal arborization and tau phosphorylation in siRNA-exposed neurons, at 24 h from gene silencing the cells were exposed to 500 μM NMDA and 100 μM glycine in Mg^{2+}-free KRS for 10 minutes. Pre-treatment with the GluN2B antagonist ifenprodil was performed in the same conditions with the addition of 10 μM ifenprodil to Mg^{2+}-free KRS 20 minutes prior to NMDA + glycine. Cells were then incubated again with their original cell culture media. A fraction of siRNA-exposed cells were subjected to media changes without the addition of NMDA and glycine as a control.

Immunocytochemistry (ICC)

For ICC cells were fixed by incubation for 15 min in 3% paraformaldehyde/3% sucrose made up in phosphate buffered saline (PBS) 1 M pH 7.4 and then stored in PBS containing 0.05% sodium azide. Slides were incubated for 10 min at 25°C in a permeabilization solution composed by 20% methanol in PBS containing 0.1% Triton X-100, than 30 min in blocking solution, composed by 2% (v/v) normal goat serum (NGS - Sigma Aldrich, Italy) plus 3% (w/v) BSA (Sigma Aldrich, Italy) in PBS containing 0.1% Triton X-100, and then over night at 4°C with primary antibody at the optimal working dilution made up in blocking solution. On the following day, cells were incubated for 1 h at 25°C with the fluorescent secondary antibody diluted in PBS containing 0.1% Triton X-100 with 0.1% BSA. For double labelling, at the end of this incubation, cells underwent another cycle of staining. Cell nuclei were counter-stained with Hoechst 2495 (Sigma Aldrich, Italy). Coverslips were then mounted on glass slides with the Vectashield mounting medium (Vector Laboratories, Burlingame, CA, USA).

Immunohistochemistry (IHC)

For IHC, mice were anesthetized with chloral hydrate (400 mg/kg, i.p.) and were perfused transcardially with 4% ice-cold paraformaldehyde in 0.1 M phosphate buffer, pH 7.2. For P0 pups, mice were decapitated and the whole head was fixed in 4% ice-cold parafolmadehyde overnight. After 4 h of post-fixation, brains were put in 18% sucrose and the day after, 30 µm coronal sections were cut with a cryostat (Leica Biosystems).

Free floating sections were washed with PBS containing 0.3% Triton X-100 and incubated for 30 min at 25°C in a permeabilization solution composed by 20% methanol in PBS containing 0.3% Triton X-100, than 1 h in blocking solution, composed by 2% (v/v) normal goat serum (NGS - Sigma Aldrich, Italy) plus 3% (w/v) bovine serum albumin (BSA - Sigma Aldrich, Italy) in PBS containing 0.3% Triton X-100, and then over night at 4°C with primary antibody at the optimal working dilution made up in blocking solution. On the following day, cells were incubated for 1 h at 25°C with the fluorescent secondary antibody diluted in PBS containing 0.3% Triton X-100 with 0.1% BSA. For

double labelling, at the end of this incubation, cells underwent another cycle of staining. Cell nuclei were counter-stained with Hoechst 2495 (Sigma Aldrich, Italy). Coverslips were then mounted on glass slides with the Vectashield mounting medium (Vector Laboratories, Burlingame, CA, USA).

Antibodies

A list of the primary antibodies used for this study is summarized in Table 1. Secondary antibodies used for IHC and ICC were anti mouse Cy3-conjugated, anti rabbit Cy3- or FITC-conjugated (Jackson ImmunoResearch, Baltimore, USA) and anti sheep ALEXA-488-conjugated (Molecular probes, Eugene, OR, USA).

Secondary antibodies used for WB were anti-mouse, anti rabbit (Santa Cruz Biotecnology, Santa Cruz, CA, USA) and anti sheep (Southern Biotech, Birminghan, AL, USA) horseradish peroxidase-conjugated.

Confocal and fluorescence microscopy

Fixed cells and mouse brain sections were observed by means of an inverted light/epifluorescence microscope (Olympus IX50; Olympus, Milan, Italy) or by means of a Zeiss confocal laser microscope (Carl Zeiss S.p.A., Milan, Italy), with the laser set on l = 405–488–543 nm and the height of the sections scanning = 1 µm. Images (512x512 pixels) were then reconstructed using LSM Image Examiner (Carl Zeiss S.p.A) and Adobe Photoshop 7.0 (Adobe system, Mountain View, CA, USA) software.

Sholl analysis

A Sholl analysis of single neurons in the primary cortical neuronal cell cultures was performed manually on the basis of the ImageJ (NIH, USA). After MAP-2 ICC randomly chosen neurons were analyzed. The number of intersections of the neurite tree with increasing circular perimeters from the

center of the soma was counted every 30 μm by usig a calibrated concentric circle mask. The collected data were plotted by using GraphPad Prism 4 and analyzed as described below.

Western Blot (WB)

For total protein extraction, either cell pellets or mouse brain tissue was lysed in a buffer containing 50 mM Tris-HCl, pH 7.4, 150 mM NaCl, 0.5% Na Deoxicolate, 0.1% Na Dodecylsufate, 2 mM ethylenediaminetetraacetic acid (EDTA), 0.1 mM Phenylmethylsulfonyl fluoride (PMSF), 1 mM N-ethylmaleimide, Na Ortovanadate 1 mM, 1% Nonidet P40, NaF 1 mM and protease inhibitor cocktail (Roche Diagnostics, Mannheim, Germany). For membrane protein extraction, cell pellets were homogenated in NP40 buffer (NaCl 150 mM, 50 mM HEPES pH 7.4, 1 % NP40) nuclei and cell debris were eliminated by centrifugation of the homogenate at 500 x g for 10 minutes at 4°C. Pellets were discarded and supernatants were then centrifuged at 100000 x g for 1 hour at 4°C. The resulting pellet was then dissolved the protein precipitate in lysis buffer and centrifuged at 100000 x g at 4°C, for 1 hour. This final pellet containing membrane fractions was used for WB analysis. Protein concentrations in the samples were measured by using the Bradford assay (Pierce, Rockford, IL, USA). Equal amounts of proteins (30 μ) were run on 4–12% Nu-PAGE NovexBis–Tris gels (Invitrogen) and blotted on a polyvinylidene difluoride (PVDF) Immobilon-P membrane (Millipore, Milan, Italy). Densitometric analysis of bands was performed by means of Gel Pro Analyzer version 6.0. (Media Cybernetics, Bethesda, MD, USA). Bands' densities were normalized to either glyceraldehyde 3-phosphate dehydrogenase (GAPDH) or α-tubulin levels as a control of equal loading of samples. For membrane protein extracts GluN1 and GluN2B bands were normalized to the membrane protein amyloid precursor protein (APP) levels as a control for equal loading.

Analysis of GluN2B, GluN1 and PSD-95 density

Images were obtained by using a Zeiss LSM510 Laser scanning confocal Microscope (Ziess, Oberkochen, Germany) with a 63 X oil-immersion objective. All images within a single experiment

were acquired using equivalent settings by an individual who was blind to treatment conditions. Neurons were selected at random from each quadrant of the coverslip by PGRN staining. For each neuron, three dendrites were chosen and their length was measured from phase contrast images. To quantify the ICC data from the 3 dendrites from each neurons, these latter were chosen randomly for image acquisition and processed using Image J imaging software (10 cells from each condition from 3 independent experiments were acquired). For each experiment, the efficiency of PGRN gene silencing was confirmed by the analysis of the ICC signal and images in each channel were captured using the same exposure time across all fixed cells. Images were acquired as grayscale from individual channels and pseudocolor overlays were prepared using Adobe Photoshop. To quantify GluN1, GluN2B and PSD-95 density per dendrite length in ICC photomicrographs, the digital images were subjected to a user-defined intensity threshold (the same thresholds sets were used for each independent experiment) to select clusters and measured for cluster intensity, number, and area for the selected region by using the Image J software. All imaging and analysis were done blind to gene silencing and treatment condition. All the measurements were normalized to control cells values.

Statistical analysis

Each experiment was replicated at least 3 times with each experimental condition produced either in duplicate or triplicate. Differences between 88 kDa and 62 kDa PGRN levels assayed by WB in cortical and hippocampal samples from control mice were analyzed by two-way ANOVA + Bonferroni's multiple comparison test. Differences in 62 kDa PGRN, GluN1 and GluN2B levels between cortical and hippocampal neurons were analyzed by Student's t-test. The effect of PGRN gene silencing on PGRN levels and LDH released was analyzed by one-way ANOVA followed by Newman-Keuls post-comparison test. The same analysis was used to evaluate differences in GluN1, GluN2B levels, intracellular Ca^{2+} load as well as GluN1, GluN2B and PSD-95 distribution in control, SCR-treated and siRNA-exposed cells. Two-way ANOVA + Bonferroni's post-comparison test was used to analyze the data from Sholl analysis.

JPET Fast Forward. Published on September 12, 2017 as DOI: 10.1124/jpet.117.242164
This article has not been copyedited and formatted. The final version may differ from this version.

Results

1. Age-related differences in the expression of the mature 62 kDa and glycosylated 88 kDa form of PGRN in cortical and hippocampal extracts of C57BL/6J mice

Since the aim of this work was to estimate the effect of PGRN reduction in primary neurons, we first probed the expression of PGRN in the cortex and hippocampus of C57BL/6J mice during aging (Fig.1A-C). By WB analysis, we found that newborn mice only express the mature non-glycosylated form of the protein of 62 kDa. The expression of this form of the protein was significantly higher in cortical extract when compared to hippocampal extracts (Fig. 1A,C). However, the expression of non-glycosylated PGRN was significantly reduced both in the hippocampus and cortex of 1, 8 and 12 month-old mice when compared to newborn mice (Fig.1A,C). In parallel, the levels of the glycosylated 88 kDa PGRN form, that was low at P0, strongly increased in the cortical and hippocampal extracts from C57BL6J mice along with aging (Fig. 1A,B). Of note, the levels of 88 kDa glycosylated PGRN in the hippocampal extracts from 12 month-old mice were found to be significantly higher than those observed in 1 and 8 month-old mice (Fig. 1A,B). Conversely, the levels of 88 kDa PGRN in the cortical extracts of 1, 8 and 12-month-old mice were comparable (Fig. 1A,B).

2. Characterization of primary cortical and hippocampal neuronal cell cultures

In order to definitively choose whether to work on cortical or hippocampal neurons we probed PGRN levels in the cell cultures prepared from newborn P0 mice by WB. In line with the above observations we found that at 10 DIV these cells only expressed the 62 kDa PGRN form and that its levels were significantly higher in cortical neurons when compared to hippocampal neurons (Fig. 2A). These findings indicated that cortical neurons may constitute a more representative model to study the effects of PGRN gene silencing “in vitro”.

Since one of our aim was to probe the effect of PGRN gene silencing on GluN2B-containing NMDAR, we also studied the levels of GluN1 and GluN2B in primary cortical and hippocampal neuronal protein extracts at DIV 10. By WB we found that the expression of GluN1 and GluN2B were significantly higher in cortical neurons when compared to hippocampal neurons (Figure 2B). These changes were not due to differences in cell maturation as confirmed by the analysis of neuronal morphology in phase contrast images (Fig. 2C) and by the fact that both cortical and hippocampal neurons showed a good degree of expression of mature neuronal markers such as NeuN (Fig. 2D), MAP-2 (Fig. 2E) and GAD-67 (Fig. 2F).

3. Experimental design and evaluation of PGRN gene silencing and cell viability

In this study we aimed at evaluating whether PGRN reduction could modulate neuronal structural plasticity through the modulation of GluN2B-containing NMDA and tau phosphorylation. For this reason we used primary cortical neurons cultured for 10 DIV prepared from newborn P0 mice (Fig. 3A). Cells were subjected to silencing RNA (siRNA)-based RNA interference at DIV 10. Four different siRNA sequences (Fig. 3B) were tested. Efficacy of PGRN gene silencing and NMDA and tau phosphorylation were evaluated at 72h from RNAi, cell viability was probed at 96h from RNAi, while neuronal morphology and GluN2B and PGRN expression was analyzed at 120h from gene silencing. A schematic representation of our experimental design is showed in Fig. 3A.

By WB we found that siRNA sequence 4 was able induce an efficient 60 % reduction of PGRN levels that was evident at 72 h from RNAi (Fig. 3C), without affecting cell viability assayed by LDH release assay at 96 h (Fig. 3D). The reduction of PGRN by siRNA 4 was confirmed by immunocitochemical analysis (Fig. 3E).

3. PGRN gene silencing reduces GluN2B-containing NMDA receptor density and expression

To evaluate whether PGRN gene silencing could influence NMDA receptors we probed whether this could change the membrane levels and density of GluN2B-containing NMDA receptors. The choice to analyze GluN2B-containing NMDA receptors was mostly related to the fact that their expression and clustering in primary cortical neurons appears to be established since DIV3 while GluN2A developmental expression and clustering are delayed and became detectable between DIV12 and DIV18 (Desai et al., 2002; Li et al., 1998; Mizuta et al., 1998). In line with these findings, we found that GluN2A was not detectable in primary cortical neurons at DIV15 (Supplementary figure 1A). The levels of GluN1 and GluN2B in the membrane protein extracts were analyzed by WB (Fig. 4A). We found that PGRN gene silencing induced a statistically significant reduction of both GluN1 (** -22.8 %; $P < 0.01$) and GluN2B levels (** -39 %; $P < 0.01$) as indicated by the reduced density of the immunopositive bands when compared to control neurons. Exposure to SCR RNA sequences did not alter GluN1 and GluN2B levels (Figure 4A). Similarly, GluN1 and GluN2B levels were found to be reduced in total protein extracts produced from siRNA-exposed primary cortical neurons when compared to either control or SCR RNA-treated cells (Supplementary figure 1B). We also probed whether silenced neurons may display decreased activation of GluN2B-containing NMDA receptors after NMDA + glycine exposure. By using the GluN2B-selective antagonist ifenprodil we found that NMDA + glycine-induced Ca^{2+} release from primary cortical neurons was GluN2B dependent (Fig. 4B). Moreover, we observed that cells exposed to PGRN gene silencing showed a decreased Ca^{2+} overflow upon NMDA stimulation (Fig. 4B). We also evaluated whether PGRN gene silencing could decrease the levels of α-amino-3-hydroxy-5-methyl-4-isoxazolepropionic acid (AMPA) receptors in primary cortical neurons. We found that the cells that were exposed to siRNA did not exhibit a decrease of GluA1 or GluA2 levels (Supplementary Figure 1C).

Then, we investigated the co-localization between NMDA receptors with either the pre-synaptic protein marker synaptophysin or the post-synaptic protein PSD-95 in primary control cortical neurons at DIV10 (Fig. 4C). The results showed that GluN2B and GluN1 mostly co-localized with the post-synaptic marker PSD-95 while NR2B only showed a modest co-localization with synaptophysin, thus

indicating that GluN2B-containing NMDA receptors were mostly localized at extra-synaptic sites (Fig. 4C). We then probed the density of GluN1, GluN2B and PSD-95 ICC at 72 h from gene silencing in neurons that were double-labelled with NMDA and PGRN to ensure that we could measure the changes in relation of PGRN levels (Fig. 4D). The densitometric analysis showed that cells that were exposed to PGRN gene silencing displayed a statistically significant reduction of GluN1 (Fig. 4E), GluN2B (Fig. 4F) and PSD-95 (Fig. 4G) density when compared to control or SCR treated cells. Finally, since it has been previously described that PGRN depletion can cause a decrease of spine density (Petkoe et al., 2012), we also assayed whether the decrease of NR1, NR2B and PSD-95 might coincide with a reduction of dendritic spines. We found that at 72 h from siRNA exposure primary neuronal cells showed a statistically significant reduction in spine density when compared to either control (*** $P < 0.001$) or SCR RNA-treated cells (°°° $P < 0.01$) (Supplementary figure 1D). These results support that the decrease of GluN2B-containing NMDAR observed after PGRN depletion was associated with a reduction of spine density.

4. PGRN gene silencing reduces neuronal arborization

Neuronal arborization was analyzed by Sholl analysis (Chen and Firestein, 2007; Kutzing et al., 2010) by evaluating the differences in the number of dendritic intersections between MAP-2-positive control, SCR-exposed- and siRNA-exposed neurons at 120 h from gene silencing. In order to assess whether GluN2B-containing NMDA receptor stimulation could be involved in the onset of the PGRN gene silencing-dependent decrease of neuronal arborization, we also analyzed siRNA-exposed cells that were subjected to acute stimulation with either NMDA + glycine or NMDA + glycine following ifenprodil pretreatment. We found that cells exposed to PGRN gene silencing showed a statistically significant decrease of dendritic intersections (Fig. 5A) at 60, 90, 120 and 150 μm from the soma (Fig. 5B). To corroborate the specificity of the effect of PGRN gene silencing on neuronal arborization we compared the effect of siRNA1, siRNA2 and siRNA3 and siRNA4 on this parameter. In line with the data deriving from the evaluation of the gene silencing efficiency of these sequences

JPET Fast Forward. Published on September 12, 2017 as DOI: 10.1124/jpet.117.242164
This article has not been copyedited and formatted. The final version may differ from this version.

we found that siRNA2 and siRNA3 induced a modest increase in neuronal arborization, while siRNA 4 significantly reduced the number of intersections at 30, 60, 90, 120 and 150 μm from the soma when compared to siRNA1 (Supplementary figure 2A,B). These observations were corroborated by data showing that the efficiency rate of PGRN gene silencing achieved by using the different siRNA sequences inversely correlated with the total numer of intersections counted for siRNA1, siRNA2, siRNA3 or siRNA4 (Supplementary figure 2C).

We then wanted to probe the effect of NMDA stimulation on neuronal arborization in siRNA4 exposed cells. Of note, an acute stimulation of cortical neurons with NMDA + glycine at 24 h from gene silencing could prevent the effect of PGRN gene silencing on neuronal arborization. Indeed, the NMDA + glycine treated PGRN-silenced neurons showed a weaker, although significant, difference in the number of dendritic intersections only at 60 and 90 μm from the soma when compared to siRNA-exposed cells. Of note, a pretreatment with the GluN2B selective antagonist ifenprodil before the acute stimulation with NMDA + glycine in siRNA-exposed cells was able to significantly prevent the effect of NMDA stimulation on neuronal arborization in the cells exposed to PGRN gene silencing. Finally, we evaluated the persistence of GluN2B decrease in MAP-2 positive cells at 120h from gene silencing in order to ensure they effectively displayed GluN2B reduction. As shown in Fig. 5C we observed a decrease of GluN2B in the siRNA-exposed MAP-2-positive cells but not in control or SCR-treated neurons.

PGRN gene silencing affects NMDA receptor-dependent tau phosphorylation

To evaluate whether PGRN gene silencing could modulate NMDA-dependent tau phosphorylation we assayed tau phosphorylation of Ser 262, 396 and 404 normalized against total tau levels probed by using the tau 46 antibody by WB (Fig. 6A).

We found that PGRN gene silencing significantly reduced the levels of tau phosphorylation in cortical neurons exposed to siRNA when compared to control or SCR RNA-treated cells. However, the acute treatment with NMDA + glycine could prevent the reduction of tau phosphorylation in siRNA-

JPET Fast Forward. Published on September 12, 2017 as DOI: 10.1124/jpet.117.242164
This article has not been copyedited and formatted. The final version may differ from this version.

exposed neurons, indicating that the abatement of tau phosphorylation was related to the decrease of NMDA receptor levels and activity observed in the cells with PGRN gene silencing.

Discussion

Collectively, our results indicate that a partial drop of PGRN affects GluN2B-containing NMDA receptor density, tau phosphorylation as well as dendritic arborization in primary mouse cortical neurons. In particular, we found that haploinsufficiency-like PGRN depletion, achieved by RNAi, could reduce GluN1 and GluN2B membrane levels and density at 72 h from gene silencing. These alterations were associated with a reduction spine density and of NMDAR-mediated Ca^{2+}-influx in primary cortical neurons that were followed by a decrease of neuronal arborization 96 h after RNAi. Notably, we found that the decrease of neuronal arborization induced by PGRN gene silencing was prevented by NMDA receptor stimulation, whose effect was in turn reverted by the GluN2B-selective antagonist ifenprodil, therefore supporting the existence of a causative link between these phenomena. Indeed, these evidences suggest that the decrease of GluN2B-containing NMDAR could mediate the negative effect of PGRN abatement on neuronal trophism. To date, in line with our data, it has been foundt that although GluN2B is not essential for dendrite growth and branching, its knockdown has been found to decrese neuronal spine density and the number of apical dendrites (Espinosa et al., 2009) thus suggesting that its action is relevant for dendrite patterning. In primary cortical neurons in culture at DIV 10 NMDA activity at excitatory synapses is ensured by the coupling of GluN1 and GluN2B that can cluster at both synaptic and extra-synaptic sites, with only a very small fraction of synaptic NMDA receptors containing the GluN2A subunit (Li et al., 1998). These findings indicate that NMDA-dependent regulation of primary cortical neurons is strictrly dependent on GluN2B-cotaining NMDA receptors. In line with this hypothesis and with our findings, their inhibition has been found to be associated with dendrite degeneration and reduced ERK1/2 kinase activation in primary neurons (Chernova et al., 2007).

Our results also showed that PGRN gene silencing could decrease GluN2B-containing NMDA-receptor-mediated tau phosphorylation at Ser 262 and PHF-1 sites. This observation suggests that PGRN haploinsufficiency, by reducing GluN2B-containing NMDAR signaling, can affect the structural plasticity of cortical neurons by modulating the ability of tau to interact with microtubules.

Indeed, as a result of reduced tau phosphorylation, microtubular networks could be impaired by stiffness and in parallel synapse formation can be hampered, thus generating the loss in neuronal connectivity that is typical for FTLD. Although further studies are needed to probe this hypothesis, it is well recognized that interaction of tau with microtubules is essential for the proper maintenance of neuronal structural plasticity and for the transport of synaptic cargoes along microtubules. The loss of efficient interaction of tau with microtubules deriving from its hyperphosphorylation is implicated in the onset of several neurodegenerative diseases affecting cortical regions including familial FTLD (Spillantini and Goedert, 2013). Proper tau activity is thus crucial for cortical neuron function and homeostasis, thus supporting that subtle changes in the post-translational modifications driving its function could severely impinge on cortical neuron resilience. In this scenario, tau hyperphosphorylation, that generates neurofibrillary tangles (NFT) in MAPT-associated FTLD and tau ipophosphorylation, resulting from PGRN reduction in FTLD with PGRN mutations, could be two opposite mechanisms that, by compromising tau-microtubular interaction, cound drive neuronal cells toward degeneration. Our results support that the reduced NMDA receptors' activity deriving from low PGRN levels could pivotally control the capacity of tau to interact with microtubules in FTLD with PGRN mutations. Notably, several previous research reports have described the occurrence of NMDA receptor-mediated tau phosphorylation in neuronal cells (Sava et al., 2012; Zhou et al., 2009) suggesting that this process could be part of a physiological intracellular signaling cascade regulating synaptic NMDA receptor-dependent transmission during structural plasticity changes. In particular, NMDA receptors can increase the phosphorylation of tau on specific sites that mediate its interaction with synaptic proteins. Moreover, the phosphorylation of tau controls the interaction of tau with the postsynaptic PSD-95-Fyn-NMDA receptor complex, that regulates GluN2B-containing NMDA-dependent synaptic plasticity, suggesting that physiologically occurring phosphorylation of tau could serve as a regulatory mechanism to prevent NMDA receptor overexcitation (Mondragon-Rodriguez et al., 2012). These findings, when coupled to our results, hint that PGRN decrease increase neuronal vulnerability by leading to a reduction of GluN2B-containing

NMDA receptors, that by affecting the rate of tau phosphorylation in turn, might pertub the ability of neuronal cells to easily display structural plasticity changes. Structural changes occur in the brain throughout life, including the generation of new neurons and other brain cells and connections between and among neurons and structural plasticity provides the mechanism for the brain to repair itself (Gage, 2004). In addition, subtle changes in functional plasticity in brain cortical areas can contribute to behavioural impairments in the absence of significant pathology (Burke and Barnes, 2006). This implies that in PGRN mutation carriers, cortical neurons holding reduced PGRN levels may present a lower ability to display structural plasticity changes. This phenomenon may also significantly decrease the resilience of to these cells to aging and stressors.

Consistently, recent findings reported that PGRN deficient mice display reduced synaptic connectivity and plasticity impairment occurring before neuropathological abnormalities (Petkau et al., 2012). Moreover, PGRN deficiency reduces synaptic pruning in the thalamus by dysregulating microglial cells (Lui et al., 2016). Our finding, show that the PGRN-deficiency-related decrease of neuronal arborisation is ascrivable to a decrease of NR2B-containing NMDA receptors that is paralleled by a decrease of spine density. These evidences sound in line with previous findings showing that, although PGRN reduction can enhance transmission at individual synapses, it decreases gross neuronal connectivity (Tapia et al., 2011) and confirm that important neuronal plasticity changes occur in the early stages of disease. Remarkably, both NMDA receptor activity and tau phosphorylation have been found to be highly involved in the control of microtubule dynamic changes during neuronal structural plasticity (Biernat and Mandelkow, 1999; Caceres and Kosik, 1990; Dawson et al., 2001; Knops et al., 1991).

Worth of note, recent finding indicates that PGRN reduction is associated with increased tau phosphorylation in P301L transgenic mice (Hosokawa et al., 2015). Although these observations are partially not in agreement with our results, which indicate that PGRN decrease reduces tau phosphorylation, it is feasible that other mechanisms may be involved in the opposite phenomenon in the transgenic P301L tau model. This is supported by the fact that PGRN deficient mice do not

JPET Fast Forward. Published on September 12, 2017 as DOI: 10.1124/jpet.117.242164
This article has not been copyedited and formatted. The final version may differ from this version.

show abnormalities in tau phosphorylation (Hosokawa et al., 2015). In addition, we cannot exclude that a partial reduction of PGRN resulting in the case of haploinsufficiency may affect neuronal homeostasis in a manner completely different than the complete absence of the protein, as supported by the different pathological phenotypes that have been described for PGRN knockout and PGRN insufficient mice (Arrant et al., 2015; Filiano et al., 2013; Martens et al., 2012; Petkau et al., 2012; Yin et al., 2010). Data in human CSF further support our experimental evidences as we previously described that tau phosphorylation is increased in AD patients and in FTLD patients compared with controls, but not in FTLD patients carrying a GRN mutation causing progranulin haploinsufficiency (Carecchio et al., 2011).

The results of this study indicate that an haploinsufficincy-like decrease of PGRN can reduce the density and activity of GluN2B-containing NMDA receptors. This phenomenon is associated with a reduction of NMDA-receptor-mediated tau phosphorylation as well as a loss of neuronal dendritic arborization, that is reverted by an acute GluN2B-containing NMDA receptors stimulation at 24 h from gene silencing. These findings support that GluN2B-containing NMDA receptors could be crucial mediators for the control of PGRN-dependent cortical neuron neurotrophism.

Collectively, these observations suggest that an aberrant regulation of GluN2B-containing NMDA receptors resulting from PGRN loss of function mutations, could impinge on cortical neuron resilience by perturbing their ability to display structural plasticity changes. The resulting progressive decline of neuronal trophism could likely initiate neurodegeneration in FTLD with GRN mutations. These observations have relevant implications for understanding the molecular mechanisms underlying the onset of FTLD.

JPET Fast Forward. Published on September 12, 2017 as DOI: 10.1124/jpet.117.242164
This article has not been copyedited and formatted. The final version may differ from this version.

Authorship Contributions

Participated in research design: Bellucci, Spano, Zaltieri.

Conducted experiments: Bellucci, Longhena, Zaltieri, Grigoletto, Faustini, La Via

Performed data analysis: Longhena, Zaltieri, Grigoletto.

Wrote or contributed to the writing of the manuscript: Bellucci, Longhena, Ghidoni, Benussi, Spano, Missale.

Conflict of interest

The authors declare that they have no conflict of interest.

Reference List

Arendt T, Stieler J, Holzer M (2015) Brain hypometabolism triggers PHF-like phosphorylation of tau, a major hallmark of Alzheimer's disease pathology. *J Neural Transm* **122**: 531-539.

Arrant AE, Patel AR, Roberson ED (2015) Effects of Exercise on Progranulin Levels and Gliosis in Progranulin-Insufficient Mice. *eNeuro*. **2**.

Baker M, Mackenzie IR, Pickering-Brown SM, Gass J, Rademakers R, Lindholm C, Snowden J, Adamson J, Sadovnick AD, Rollinson S, Cannon A, Dwosh E, Neary D, Melquist S, Richardson A, Dickson D, Berger Z, Eriksen J, Robinson T, Zehr C, Dickey CA, Crook R, McGowan E, Mann D, Boeve B, Feldman H, Hutton M. (2006) Mutations in progranulin cause tau-negative frontotemporal dementia linked to chromosome 17. *Nature* **442**: 916-919.

Benussi L, Ciani M, Tonoli E, Morbin M, Palamara L, Albani D, Fusco F, Forloni G, Glionna M, Baco M, Paterlini A, Fostinelli S, Santini B, Galbiati E, Gagni P, Cretich M, Binetti G, Tagliavini F, Prosperi D, Chiari M, Ghidoni R. (2016) Loss of exosomes in progranulin-associated frontotemporal dementia. *Neurobiol Aging*. **40**: 41-49.

Biernat J and Mandelkow EM (1999) The development of cell processes induced by tau protein requires phosphorylation of serine 262 and 356 in the repeat domain and is inhibited by phosphorylation in the proline-rich domains. *Mol Biol Cell* **10**: 727-740.

Borroni B, Alberici A, Cercignani M, Premi E, Serra L, Cerini C, Cosseddu M, Pettenati C, Turla M, Archetti S, Gasparotti R, Caltagirone C, Padovani A, Bozzali M (2012) Granulin mutation drives brain damage and reorganization from preclinical to symptomatic FTLD. *Neurobiol Aging* **33**: 2506-2520.

Bozzali M, Battistoni V, Premi E, Alberici A, Giulietti G, Archetti S, Turla M, Gasparotti R, Cercignani M, Padovani A, Borroni B (2013) Structural brain signature of FTLD driven by Granulin mutation. *J Alzheimers Dis* **33**: 483-494.

Burke SN and Barnes CA (2006). Structural plasticity in the aging brain. *Nat Rev Neurosci*. **7**, 30-40.

Caceres A. and Kosik KS (1990). Inhibition of neurite polarity by tau antisense oligonucleotides in primary cerebellar neurons. *Nature* **343**: 461-463.

Carecchio M, Fenoglio C, Cortini F, Comi C, Benussi L, Ghidoni R, Borroni B, De Riz M, Serpente M, Cantoni C, Franceschi M, Albertini V, Monaco F, Rainero I, Binetti G, Padovani A, Bresolin N, Scarpini E, Galimberti D. (2011) Cerebrospinal fluid biomarkers in Progranulin mutations carriers. *J Alzheimers Dis* **27**: 781-90.

Carpenter-Hyland EP and Chandler LJ (2007) Adaptive plasticity of NMDA receptors and dendritic spines: implications for enhanced vulnerability of the adolescent brain to alcohol addiction. *Pharmacol Biochem Behav* **86**: 200-208.

Chen H and Firestein BL (2007) RhoA regulates dendrite branching in hippocampal neurons by decreasing cypin protein levels. *J Neurosci* **27**: 8378-86.

Chernova T, Steinert JR, Guerin CJ, Nicotera P, Forsythe ID, Smith AG (2007) Neurite degeneration induced by heme deficiency mediated via inhibition of NMDA receptor-dependent extracellular signal-regulated kinase 1/2 activation. *J Neurosci* **27**: 8475-85.

Chitramuthu BP, Baranowski DC, Kay DG, Bateman A, Bennett HP (2010) Progranulin modulates zebrafish motoneuron development in vivo and rescues truncation defects associated with knockdown of Survival motor neuron 1. *Mol Neurodegener* **5**: 41.

Cruts M, Gijselinck I, van der Zee J, Engelborghs S, Wils H, Pirici D, Rademakers R, Vandenberghe R, Dermaut B, Martin JJ, van Duijn C, Peeters K, Sciot R, Santens P, De Pooter T, Mattheijssens M, Van den Broeck M, Cuijt I, Vennekens K, De Deyn PP, Kumar-Singh S, Van Broeckhoven C. (2006) Null mutations in progranulin cause ubiquitin-positive frontotemporal dementia linked to chromosome 17q21. *Nature* **442**: 920-924.

Dawson HN, Ferreira A, Eyster MV, Ghoshal N, Binder LI, Vitek MP (2001) Inhibition of neuronal maturation in primary hippocampal neurons from tau deficient mice. *J Cell Sci* **114**: 1179-1187.

Desai A, Turetsky D, Vasudevan K, Buonanno A (2002) Analysis of transcriptional regulatory sequences of the N-methyl-D-aspartate receptor 2A subunit gene in cultured cortical neurons and transgenic mice. J Biol Chem. **277**: 46374-84.

El Gaamouch F., Buisson A, Moustie O, Lemieux M, Labrecque S, Bontempi B, De KP, Nicole O (2012) Interaction between alphaCaMKII and GluN2B controls ERK-dependent plasticity. *J Neurosci* **32**: 10767-10779.

Espinosa JS1, Wheeler DG, Tsien RW, Luo L (2009) Uncoupling dendrite growth and patterning: single-cell knockout analysis of NMDA receptor 2B. *Neuron* **62**: 205-17.

Filiano AJ, Martens LH, Young AH, Warmus BA, Zhou P, az-Ramirez G, Jiao J, Zhang Z, Huang EJ, Gao FB, Farese RV, Jr., Roberson ED (2013) Dissociation of frontotemporal dementia-related deficits and neuroinflammation in progranulin haploinsufficient mice. *J Neurosci* **33**: 5352-5361.

Finch N, Baker M, Crook R, Swanson K, Kuntz K, Surtees R, Bisceglio G, Rovelet-Lecrux A, Boeve B, Petersen RC, Dickson DW, Younkin SG, Deramecourt V, Crook J, Graff-Radford NR, Rademakers R. (2009) Plasma progranulin levels predict progranulin mutation status in frontotemporal dementia patients and asymptomatic family members. *Brain* **132**: 583-591.

Gage FH (2004) Structural plasticity of the adult brain. *Dialogues Clin Neurosci* **6**: 135-141.

Ghidoni R, Benussi L, Glionna M, Franzoni M, Binetti G. (2008) Low plasma progranulin levels predict progranulin mutations in frontotemporal lobar degeneration. *Neurology* **71**: 1235-1239.

Ghidoni R, Paterlini A, Albertini V, Binetti G, Benussi L. (2012) Losing protein in the brain: the case of progranulin. *Brain Res.* **1476**: 172-82.

Gijselinck I, van der ZJ, Engelborghs S, Goossens D, Peeters K, Mattheijssens M, Corsmit E, Del-Favero J, De Deyn PP, Van BC, Cruts M (2008) Progranulin locus deletion in frontotemporal dementia. Hum Mutat **29**: 53-58.

Hosokawa M, Arai T, Masuda-Suzukake M, Kondo H, Matsuwaki T, Nishihara M, Hasegawa M, Akiyama H (2015) Progranulin reduction is associated with increased tau phosphorylation in P301L tau transgenic mice. *J Neuropathol Exp Neurol* **74**: 158-165.

Jian J, Konopka J, Liu C (2013) Insights into the role of progranulin in immunity, infection, and inflammation. *J Leukoc Biol* **93**: 199-208.

Knops J, Kosik KS, Lee G, Pardee JD, Cohen-Gould L, McConlogue L (1991) Overexpression of tau in a nonneuronal cell induces long cellular processes. J Cell Biol **114**: 725-733.

Kutzing MK, Langhammer CG, Luo V, Lakdawala H, Firestein BL (2010) Automated Sholl analysis of digitized neuronal morphology at multiple scales. J Vis Exp. **45**

Laird AS, Van HA, De ML, Timmers M, Van Den BL, Van DP, Robberecht W (2010) Progranulin is neurotrophic in vivo and protects against a mutant TDP-43 induced axonopathy. *PLoS One* **5**: e13368.

Laulagnier K, Javalet C, Hemming FJ, Sadoul R. (2017) Purification and Analysis of Exosomes Released by Mature Cortical Neurons Following Synaptic Activation. *Methods Mol Biol.* **1545**: 129-138.

Laurier-Laurin ME, De MA, Attiori ES, Cyr M, Massicotte G (2014) Blockade of lysosomal acid ceramidase induces GluN2B-dependent Tau phosphorylation in rat hippocampal slices. *Neural Plast* **2014**: 196812.

Li JH, Wang YH, Wolfe BB, Krueger KE, Corsi L, Stocca G, Vicini S (1998) Developmental changes in localization of NMDA receptor subunits in primary cultures of cortical neurons. *Eur J Neurosci* **10**: 1704-1715.

Lui H, Zhang J, Makinson SR, Cahill MK, Kelley KW, Huang HY, Shang Y, Oldham MC, Martens LH, Gao F, Coppola G, Sloan SA, Hsieh CL, Kim CC, Bigio EH, Weintraub S, Mesulam MM, Rademakers R, Mackenzie IR, Seeley WW, Karydas A, Miller BL, Borroni B, Ghidoni R, Farese RV Jr, Paz JT, Barres BA, Huang EJ (2016) Progranulin Deficiency Promotes

Circuit-Specific Synaptic Pruning by Microglia via Complement Activation. *Cell* **165**: 921-935.

Martens LH, Zhang J, Barmada SJ, Zhou P, Kamiya S, Sun B, Min SW, Gan L, Finkbeiner S, Huang EJ, Farese RV, Jr. (2012) Progranulin deficiency promotes neuroinflammation and neuron loss following toxin-induced injury. *J Clin Invest* **122**: 3955-3959.

McKhann GM, Albert MS, Grossman M, Miller B, Dickson D, Trojanowski JQ (2001) Clinical and pathological diagnosis of frontotemporal dementia: report of the Work Group on Frontotemporal Dementia and Pick's Disease. *Arch Neurol* **58**: 1803-1809.

Mizuta I, Katayama M, Watanabe M, Mishina M, Ishii K (1998) Developmental expression of NMDA receptor subunits and the emergence of glutamate neurotoxicity in primary cultures of murine cerebral cortical neurons. *Cell Mol Life Sci* **54**: 721-725.

Mondragon-Rodriguez S, Trillaud-Doppia E, Dudilot A, Bourgeois C, Lauzon M, Leclerc N, Boehm J (2012) Interaction of endogenous tau protein with synaptic proteins is regulated by N-methyl-D-aspartate receptor-dependent tau phosphorylation. *J Biol Chem* **287**: 32040-32053.

Mony L, Kew JN, Gunthorpe MJ, Paoletti P (2009) Allosteric modulators of NR2B-containing NMDA receptors: molecular mechanisms and therapeutic potential. *Br J Pharmacol* **157**:1301-1317.

Moretti DV, Benussi L, Fostinelli S, Ciani M, Binetti G, Ghidoni R. (2016) Progranulin Mutations Affects Brain Oscillatory Activity in Fronto-Temporal Dementia. *Front Aging Neurosci* **8**:35.

Petkau TL, Neal SJ, Orban PC, MacDonald JL, Hill AM, Lu G, Feldman HH, Mackenzie IR, Leavitt BR (2010) Progranulin expression in the developing and adult murine brain. *J Comp Neurol* **518**: 3931-3947.

Petkau TL, Neal SJ, Milnerwood A, Mew A, Hill AM, Orban P, Gregg J, Lu G, Feldman HH, Mackenzie IR, Raymond LA, Leavitt BR (2012) Synaptic dysfunction in progranulin-deficient mice. *Neurobiol Dis* **45**: 711-722.

Petkau TL and Leavitt BR (2014) Progranulin in neurodegenerative disease. *Trends Neurosci* **37**: 388-398.

Petkau TL, Hill A, Leavitt BR (2016) Core neuropathological abnormalities in progranulin-deficient mice are penetrant on multiple genetic backgrounds. *Neuroscience* **315**:175-195.

Pievani M, Paternico D, Benussi L, Binetti G, Orlandini A, Cobelli M, Magnaldi S, Ghidoni R, Frisoni GB (2014) Pattern of structural and functional brain abnormalities in asymptomatic granulin mutation carriers. *Alzheimers Dement* **10**: S354-S363.

Rohrer JD, Geser F, Zhou J, Gennatas ED, Sidhu M, Trojanowski JQ, Dearmond SJ, Miller BL, Seeley WW (2010) TDP-43 subtypes are associated with distinct atrophy patterns in frontotemporal dementia. *Neurology* **75**: 2204-2211.

Rohrer JD, Warren JD, Fox NC, Rossor MN (2013) Presymptomatic studies in genetic frontotemporal dementia. *Rev Neurol* (Paris) **169**: 820-824.

Rohrer JD, Nicholas JM, Cash DM, van Swieten J, Dopper E, Jiskoot L, van Minkelen R, Rombouts SA, Cardoso MJ, Clegg S, Espak M, Mead S, Thomas DL, De Vita E, Masellis M, Black SE, Freedman M, Keren R, MacIntosh BJ, Rogaeva E, Tang-Wai D, Tartaglia MC, Laforce R Jr, Tagliavini F, Tiraboschi P, Redaelli V, Prioni S, Grisoli M, Borroni B, Padovani A, Galimberti D, Scarpini E, Arighi A, Fumagalli G, Rowe JB, Coyle-Gilchrist I, Graff C, Fallström M, Jelic V, Ståhlbom AK, Andersson C, Thonberg H, Lilius L, Frisoni GB, Pievani M, Bocchetta M, Benussi L, Ghidoni R, Finger E, Sorbi S, Nacmias B, Lombardi G, Polito C, Warren JD, Ourselin S, Fox NC, Rossor MN, Binetti G. (2015) Presymptomatic cognitive and neuroanatomical changes in genetic frontotemporal dementia in the Genetic Frontotemporal dementia Initiative (GENFI) study: a cross-sectional analysis. *Lancet Neurol* **14**: 253-62.

Ryan CL, Baranowski DC, Chitramuthu BP, Malik S, Li Z, Cao M, Minotti S, Durham HD, Kay DG, Shaw CA, Bennett HP, Bateman A (2009) Progranulin is expressed within motor neurons and promotes neuronal cell survival. *BMC Neurosci* **10**: 130.

Sava A, Formaggio E, Carignani C, Andreetta F, Bettini E, Griffante C (2012) NMDA-induced ERK signalling is mediated by NR2B subunit in rat cortical neurons and switches from positive to negative depending on stage of development. *Neuropharmacology* **62**: 925-932.

Skoglund L, Matsui T, Freeman SH, Wallin A, Blom ES, Frosch MP, Growdon JH, Hyman BT, Lannfelt L, Ingelsson M, Glaser A (2011) Novel progranulin mutation detected in 2 patients with FTLD. *Alzheimer Dis Assoc Disord* **25**: 173-178.

Sleegers K, Brouwers N, Van Damme P, Engelborghs S, Gijselinck I, van der Zee J, Peeters K, Mattheijssens M, Cruts M, Vandenberghe R, De Deyn PP, Robberecht W, Van Broeckhoven C. (2009) Serum biomarker for progranulin-associated frontotemporal lobar degeneration. *Ann Neurol* **65**: 603-609.

Spillantini MG and Goedert M (2013) Tau pathology and neurodegeneration. *Lancet Neurol* **12**: 609-622.

Stein IS, Gray JA, Zito K (2015) Non-Ionotropic NMDA Receptor Signaling Drives Activity-Induced Dendritic Spine Shrinkage. *J Neurosci* **35**: 12303-12308.

Tackenberg C, Grinschgl S, Trutzel A, Santuccione AC, Frey MC, Konietzko U, Grimm J, Brandt R, Nitsch RM (2013) NMDA receptor subunit composition determines beta-amyloid-induced neurodegeneration and synaptic loss. *Cell Death Dis* **4**: e608.

Tapia L, Milnerwood A, Guo A, Mills F, Yoshida E, Vasuta C, Mackenzie IR, Raymond L, Cynader M, Jia W, Bamji SX (2011) Progranulin deficiency decreases gross neural connectivity but enhances transmission at individual synapses. *J Neurosci* **31**:11126-11132.

Van Damme P, Van HA, Lambrechts D, Vanacker P, Bogaert E, van SJ, Carmeliet P, Van Den BL, Robberecht W (2008) Progranulin functions as a neurotrophic factor to regulate neurite outgrowth and enhance neuronal survival. *J Cell Biol* **181**:37-41.

Whitwell, J.L., et al., 2007. Voxel-based morphometry in frontotemporal lobar degeneration with ubiquitin-positive inclusions with and without progranulin mutations. *Arch Neurol* **64**: 371-376.

Williams JM, Guévremont D, Kennard JT, Mason-Parker SE, Tate WP, Abraham WC (2003) Long-term regulation of N-methyl-D-aspartate receptor subunits and associated synaptic proteins following hippocampal synaptic plasticity. *Neuroscience* **118**:1003-1013.

Wyllie DJ, Livesey MR, Hardingham GE (2013) Influence of GluN2 subunit identity on NMDA receptor function. *Neuropharmacology* **74**: 4-17.

Yin F, Banerjee R, Thomas B, Zhou P, Qian L, Jia T, Ma X, Ma Y, Iadecola C, Beal MF, Nathan C, Ding A (2010) Exaggerated inflammation, impaired host defense, and neuropathology in progranulin-deficient mice. *J Exp Med* **207**: 117-128.

Zhou X, Moon C, Zheng F, Luo Y, Soellner D, Nunez JL, Wang H (2009) N-methyl-D-aspartate-stimulated ERK1/2 signaling and the transcriptional up-regulation of plasticity-related genes are developmentally regulated following in vitro neuronal maturation. *J Neurosci Res* **87**: 2632-2644.

Footnotes

This work was supported by the Fondazione Cariplo Project 2009-2633, and by the Italian Ministry of University and Reaserch, Ex 60%.

We are grateful to Prof. Alessandro Barbon for kindly providing the GluN2A, GluA1 and GluA2 antibodies.

Figure legends

Figure 1 Levels and distribution of PGRN in the cortex and hippocampus of C57BL/6J mice during aging.

A.Representative WB images showing the levels of 62 kDa and 88 kDa PGRN in the hippocampus and cortex of newborn (P0), 1 month- (1 mo), 8 month (8 mo) and 12 month-old (12 mo) mice. GAPDH bands are shown as a control of sample loading.

B. The histogram is showing the mean + s.e.m. optical density (o.d.) of the 88 kDa PGRN-immunopositive bands when normalized to GAPDH bands o.d. Please note the statistically significant increase of 88 kDa hippocampal and cortical PGRN during mouse aging. * $P < 0.05$ vs P0, ** $P < 0.01$ vs P0, • $P< 0.05$ vs 1 and 8 mo, ♦ $P< 0.001$ vs P0, Two-way ANOVA plus Bonferroni's post-comparison tets (N = 4 triplicates for each of the experimental conditions analyzed).

C. Histogram showing the relative o.d. (mean + s.e.m.) of 62 kDa PGRN-immunopositive bands when normalized to o.d of GAPDH bands. A statistically significant decrease of the protein in cortical and hippocampal neurons during mouse aging was evident. * $P < 0.001$ vs P0; ♦ $P < 0.001$ vs P0, Two-way ANOVA plus Bonferroni's post-comparison tets (N = 4 triplicates for each of the experimental conditions analyzed).

Figure 2 PGRN and GluN2B-containing NMDA receptors levels and maturation of primary cortical and hippocampal neuronal cells at 10 DIV.

A. Histogram showing the levels of 62 kDa PGRN (mean + s.e.m.) in primary mouse cortical and hippocampal neurons. Representative immunoblotting bands are shown below the bars. Please note that cortical neurons express higher levels of the protein ** $P < 0.01$ Student's T-test (N = 5 triplicates for each group).

B. GluN1 and GluN2B levels in primary mouse cortical and hippocampal neuronal cell cultures. Representative immunoblottings are shown on the left. The histograms show that GluN1 and GluN2B

levels (mean + s.e.m.) were significantly higher in cortical neurons than in hippocampal neurons * P < 0.001 Student's t-test (N = 4 triplicates for each experimental condition analyzed).

C. Phase contrast images showing the morphology of cortical and hippocampal neuronal cells at 10 DIV. Scale bar: 280 μm.

D. NeuN ICC shows the presence of mature NeuN-positive neurons in both primary cortical and hippocampal neuronal cell cultures. Scale bar: 120 μm.

E. MAP-2 immunopositivity in cortical and hippocampal neurons. Scale Bar: 50 μm.

F. GAD-67 ICC shows the presence of mature gabaergic neurons. Scale Bar: 100 μm.

Figure 3 Evaluation of PGRN gene silencing efficiency

A. Schematic diagram showing the time course of the study addressing the effect of PGRN gene silencing in primary cortical neurons.

B. siRNA sequences tested to induce PGRN gene silencing in mouse primary cortical neurons.

C. Histogram showing the efficiency of PGRN gene silencing evaluated as % decrease of protein levels in relation to control cells as measured by WB. Please note that siRNA sequence number 4 was able to induce the highest degree of PGRN gene silencing when compared to both control (CTR) and SCR-treated neurons; **P < 0.01 -60 % vs CTR, ••P < 0.01 - 55% vs SCR. This difference was also statistically significant against siRNA 1 (○ P < 0.01) and siRNA 2 and 3 (□ P < 0.05). Indeed, while siRNA1 didn't significantly reduced PGRN levels, siRNA 2 and siRNA3 induced only a modest although significant reduction of PGRN levels when compared to either control or scr-treated cells, respectively (* P < 0.05 vs CTR; • P < 0.01 vs SCR, one-way ANOVA + Neumann-Keuls post-comparison tets with N = 3 triplicates for each experimental condition analyzed.

D. Histogram showing the % LDH release in relation to control samples as a measure of cell viability and showing that siRNA sequence 4 didn't significantly increased LDH release from primary

neuronal cells when compared to either control or SCR-treated cells (one-way ANOVA + Neumann-Keuls post-comparison tets with N = 3 triplicates for each experimental condition analyzed)

E. Representative photomicrographs showing fluorescence PGRN immunoreactivity in primary mouse cortical neurons in basal condition (CTR) after exposure to non-silencing SCR RNA or siRNA sequence number 4 (siRNA4). Please note the decrease of PGRN immunopositivity in the cells exposed to siRNA4 that is indicative of the specificity of the PGRN signal and of the efficiency of silencing of this specific siRNA. Scale bar: 100 μm.

Figure 4 GluN2B-containing NMDA levels and distribution in control, SCR and siRNA exposed primary mouse cortical neurons at 72 h from gene silencing

A. Representative WB images showing GluN1, GluN2B and APP-immunopositive WB bands from membrane protein extracts of control (CTR), SCR- or siRNA-exposed neurons are shown on the left. The histograms are showing the quantification of WB immunopositive bands (mean + s.d.) for GluN1 and GluN2B proteins when normalized against APP as a reference membrane protein. ** $P < 0.01$ vs ctr, One way ANOVA + Newman-Keuls post comparison test (N = 5 triplicates for each experimental condition analyzed).

B. Histogram showing the % changes (mean % vs CTR + s.d.) in intracellular Ca^{2+} concentration observed in control, scrambe- or siRNA-exposed cortical neurons at 72 h from RNAi after NMDA + glycine stimulation. PGRN deficient cells show a statistically significant reduction of NMDA-induced Ca^{2+} overflow when compared to both control or SCR-treated neurons (** $P < 0.01$ vs CTR; •• $P < 0.01$ vs SCR, One way ANOVA + Newman-Keuls post comparison test with N = 5 triplicates for each experimental condition analyzed).

C. Representative photomicrographs showing GluN2B/Synaptophysin, GluN1/PSD-95 and GluN2B/PSD-95 double labeling in primary cortical neurons in basal condition. Please note that

GluN2B mis-localizes with the presynaptic marker synaptophysin while it co-localizes with the post-synaptic protein PSD-95. Scale bars: upper panel 40 μm, lower panel 20 μm.

D. Representative photomicropraphs showing PGRN/GluN2B double fluorescence immunolabeling in control SCR- or siRNA-exposed primary mouse cortical neurons. Please note the decrease of both proteins in the neurons exposed to siRNA. Scale bar: 90 μm.

E. GluN1 subunit distribution in primary cortical neurons in the different experimental conditions analysed at 72 h from gene silencing. Please note the statistically significant reduction of GluN1 density along neuronal processes in the siRNA-exposed cells when compared to both control or SCR-treated neurons that is evident in the histogram showing the densitometric analysis (** $P < 0.01$ vs CTR and •• $P < 0.01$ vs SCR, One way ANOVA + Newman Keuls, N = 10 triplicates for each experimental condition analyzed). Scale bar: 20 μm.

F. Density of GluN2B along neuronal processes. Please note its statistically significant decrease in the cells exposed to PGRN gene silencing when compared to control or SCR-exposed neurons. (** $P < 0.01$ vs CTR and •• $P < 0.01$ vs SCR, One way ANOVA + Newman Keuls, N = 10 triplicates for each experimental condition analyzed). Scale bar: 20 μm.

G. PSD-95 distribution. Please note the significant decrease of PSD-95 density in the cells exposed to PGRN gene silencing when compared to either CTR or SCR-treated cells (* $P < 0.05$ vs CTR and • $P < 0.05$ vs SCR, One way ANOVA + Newman Keuls, N = 10 triplicates for each experimental condition analyzed). Scale bar: 20 μm.

Figure 5 Analysis of MAP-2-positive cell arborization in primary cortical neurons

A. Immunofluorescence images showing PGRN/MAP-2 double labeling in CTR, SCR- and siRNA-exposed cells. A fraction of siRNA exposed cells was subjected to NMDA + glycine or ifenprodil (ifen) + NMDA + glycine treatment. Please note that siRNA exposed neurons show a decrease of neuronal arborization when compared to CTR or SCR-treated neurons. Silenced neurons that were

treated with NMDA + glycine appeared morphologically similar to controls. However, cells subjected to ifenprodil pretreatment prior NMDA + glycine stimulation were similar to siRNA-exposed neurons. Scale bar: 90 μm.

B. The graph is showing the results of the Scholl analysis. Please note that although siRNA-exposed neurons showed a statistically significant decrease in the number of intersections when compared to both CTR and SCR-exposed neurons, in the silenced cells that were subjected to the acute NMDA + glycine (Gly) treatment the arborization was not decreased. The protective effect of NMDA + Gly stimulation was prevented by the treatment with the GluN2B selective antagonist ifenprodil (Ifen). • $P < 0.05$ vs CTR, § $P < 0.05$ vs SCR, ○ $P < 0.05$ vs CTR, ♦ $P < 0.05$ vs SCR, + $P < 0.05$ vs siRNA, *** $P < 0.001$ vs CTR, ### $P < 0.001$ vs SCR Two way ANOVA + Bonferroni's post-comparison test, N = 6 triplicates for each experimental condition analyzed.

C. Representative photomicrographs showing MAP-2/GluNB double labeling in control, SCR or siRNA-exposed primary cortical neurons at 96 h from RNAi. Please note the lower GluN2B-immunopositive signal in the siRNA exposed cells. Scale bar: 90 μm.

Figure 6 PGRN gene silencing reduces NMDA-mediated tau phosphorylation

A. Representative immunoblotting showing PGRN, PHF-1 (Serine 396/404), Serine 262 phosphorylated and total (Tau46-positive) tau. Glyceraldehyde 3-phosphate dehydrogenase-positive bands are reported as a control for equal loading.

B. Histogram showing the quantification of PHF-1-immunopositive bands when normalized vs Tau46-immunopositive bands. Please note the statistically significant decrease of PHF-1-positive tau in siRNA exposed neurons when compared to control (** $P < 0.01$) and SCR-exposed (♦♦ $P < 0.01$ vs SCR) cells. This effect was prevented in NMDA + glycine treated cells that showed a significant increase of tau phosphorylation when compared to SCR-exposed neurons (• $P < 0.05$ One way ANOVA + Newman Keuls post-comparison test).

JPET Fast Forward. Published on September 12, 2017 as DOI: 10.1124/jpet.117.242164
This article has not been copyedited and formatted. The final version may differ from this version.

C. NMDA treatment could also prevent the statistically significant reduction of serine 262 tau phosphorylation induced by PGRN gene silencing (** $P < 0.01$ vs CTR; ♦♦ $P < 0.01$ vs SCR, One way ANOVA + Newman Keuls post-comparison test).

JPET Fast Forward. Published on September 12, 2017 as DOI: 10.1124/jpet.117.242164
This article has not been copyedited and formatted. The final version may differ from this version.

Table 1. List of the primary antibodies used for WB, ICC and IHC

Antibody	Specificity	Source	Dilution			Host
			WB	ICC	IHC	
PGRN	AA 18-589	R&D System	1:500	1:400	1:500	Sheep
APP	N-terminal	Millipore	1:500	-	-	Mouse
CD11b	-	AbD Serotec	-	-	1:1000	Rat
GAD-67	-	Millipore	-	1:1000	-	Mouse
GAPDH		Millipore	1:5000	-		Mouse
GFAP	-	DAKO	-	-	1:500	Rabbit
MAP-2		Millipore	-	1:300	-	Rabbit
GluN1	C-terminal	Santa Cruz Biotechnology	1:1500	-	-	Rabbit
GluN2B	C-terminal	Santa Cruz Biotechnology	1:1500	-	-	Rabbit
PHF1	$Tau^{pS396/pS404}$	P. Davies	1:1000	-	-	
PSD-95		Cell Signaling Technolgy	-	1:1000	-	Mouse
p-TAU(Ser262)	Tau^{pS262}	Santa Cruz Biotechnology	1:1000	-	-	Rabbit
Tau46	C-terminal	Cell Signaling Technolgy	1:1000	-	-	Mouse
Alpha-Tubulin		Sigma-Aldrich	1:5000	-	-	Mouse

JPET Fast Forward. Published on September 12, 2017 as DOI: 10.1124/jpet.117.242164
This article has not been copyedited and formatted. The final version may differ from this version.

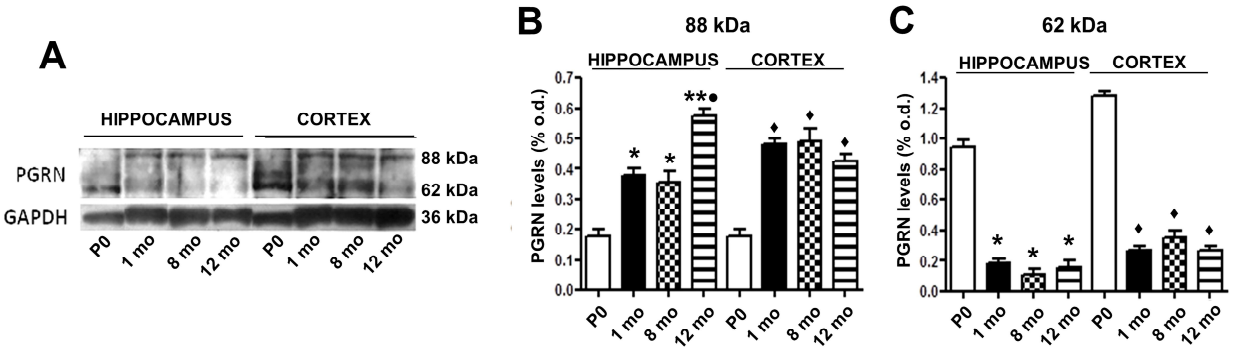

Figure 1

JPET Fast Forward. Published on September 12, 2017 as DOI: 10.1124/jpet.117.242164
This article has not been copyedited and formatted. The final version may differ from this version.

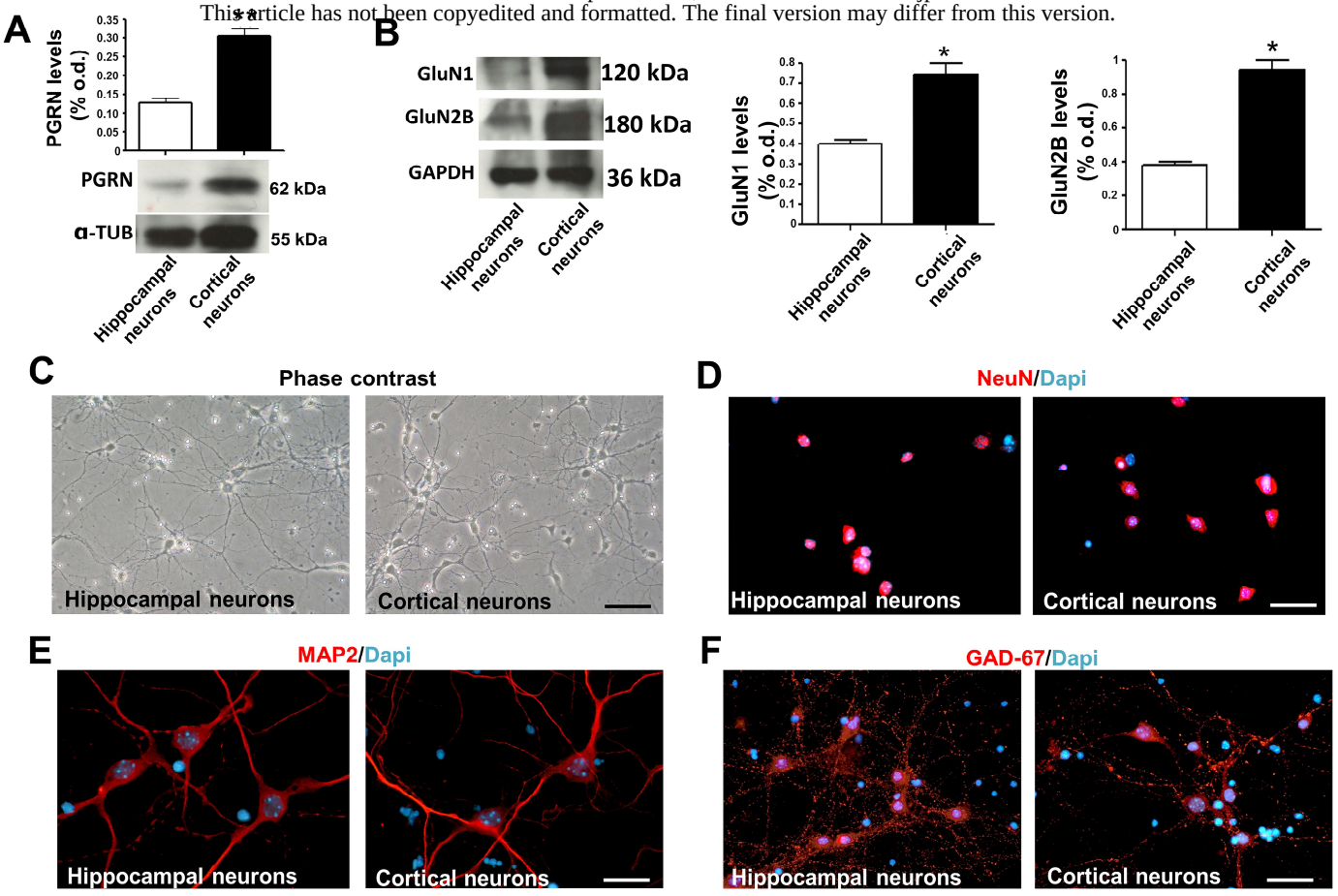

Figure 2

JPET Fast Forward. Published on September 12, 2017 as DOI: 10.1124/jpet.117.242164
This article has not been copyedited and formatted. The final version may differ from this version.

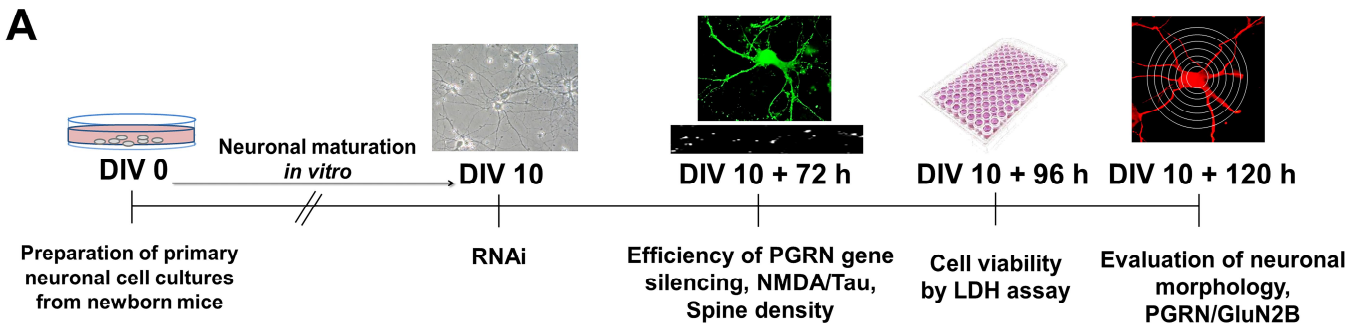

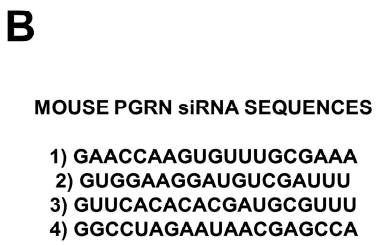

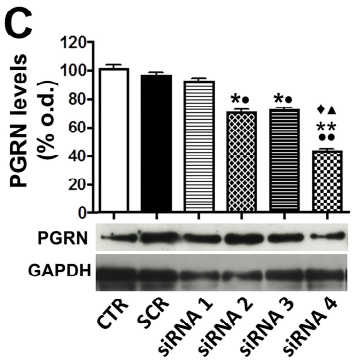

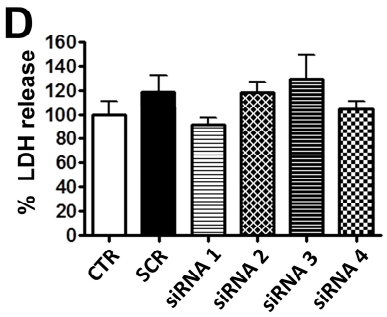

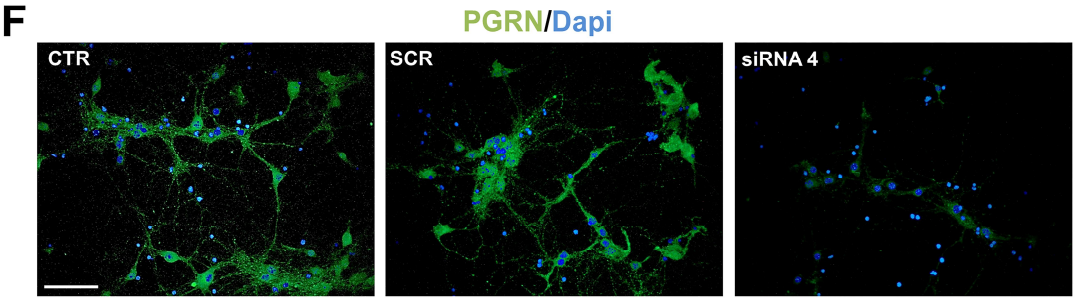

Figure 3

JPET Fast Forward. Published on September 12, 2017 as DOI: 10.1124/jpet.117.242164
This article has not been copyedited and formatted. The final version may differ from this version.

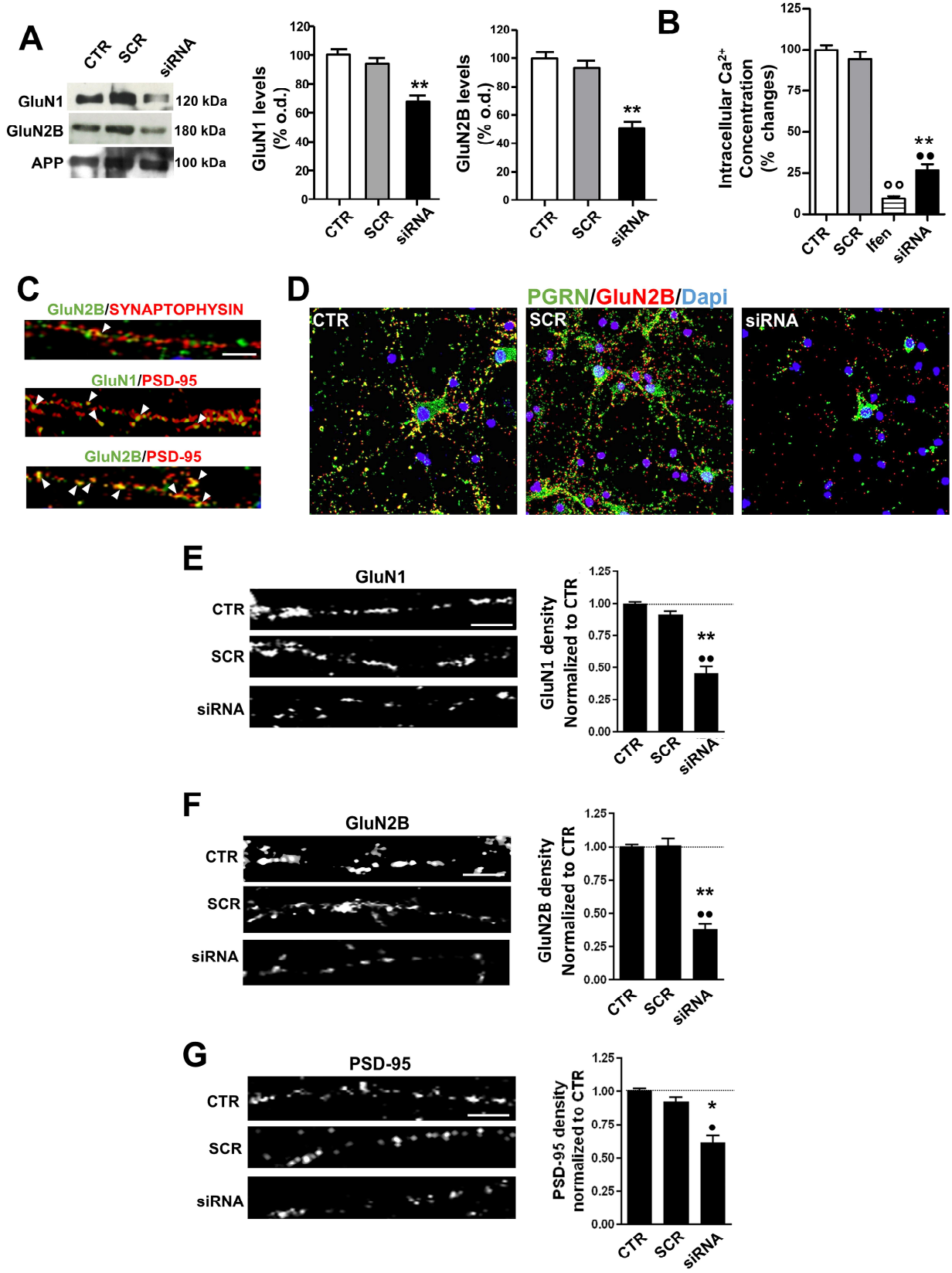

Figure 4

JPET Fast Forward. Published on September 12, 2017 as DOI: 10.1124/jpet.117.242164
This article has not been copyedited and formatted. The final version may differ from this version.

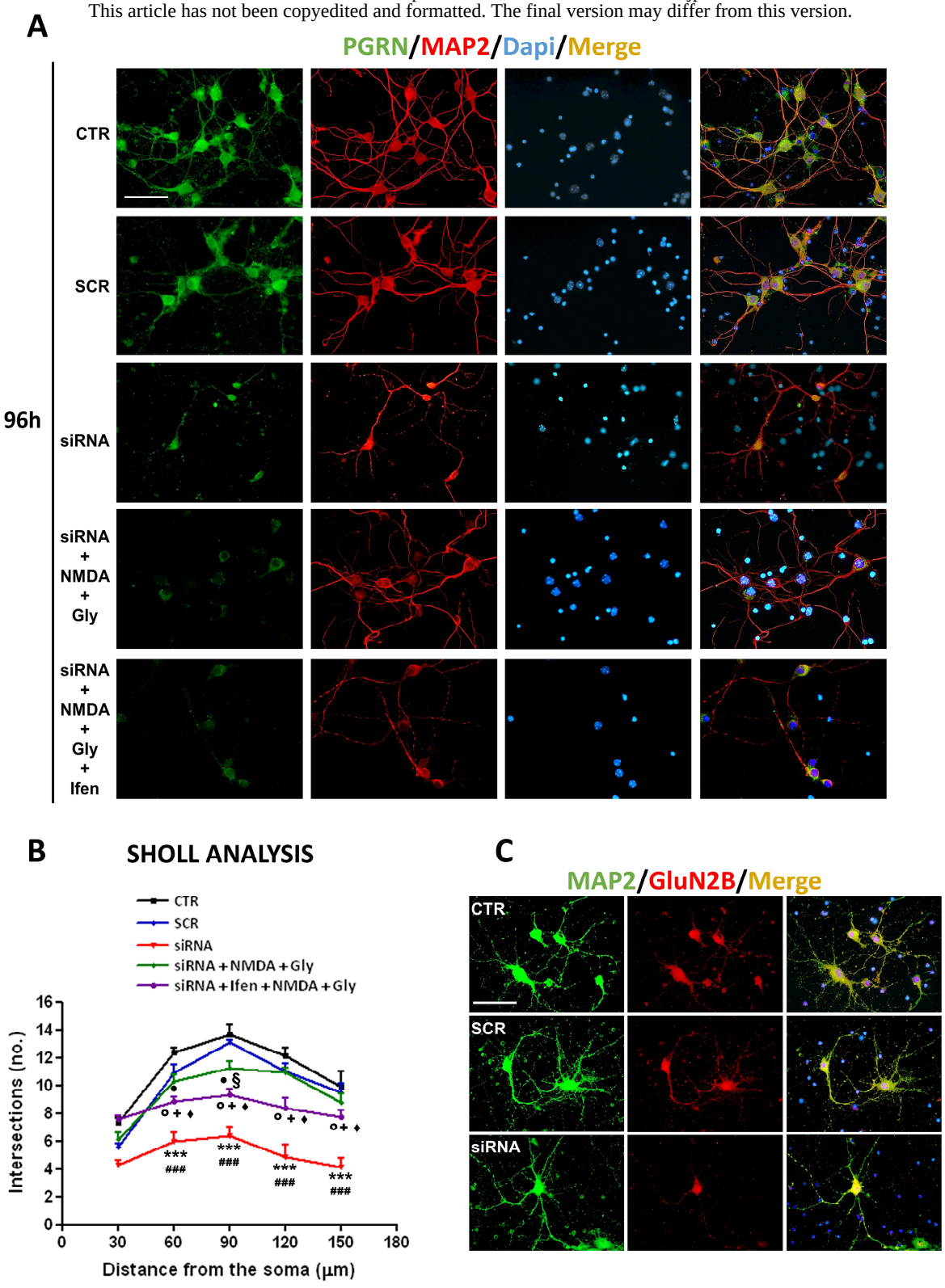

Figure 5

JPET Fast Forward. Published on September 12, 2017 as DOI: 10.1124/jpet.117.242164
This article has not been copyedited and formatted. The final version may differ from this version.

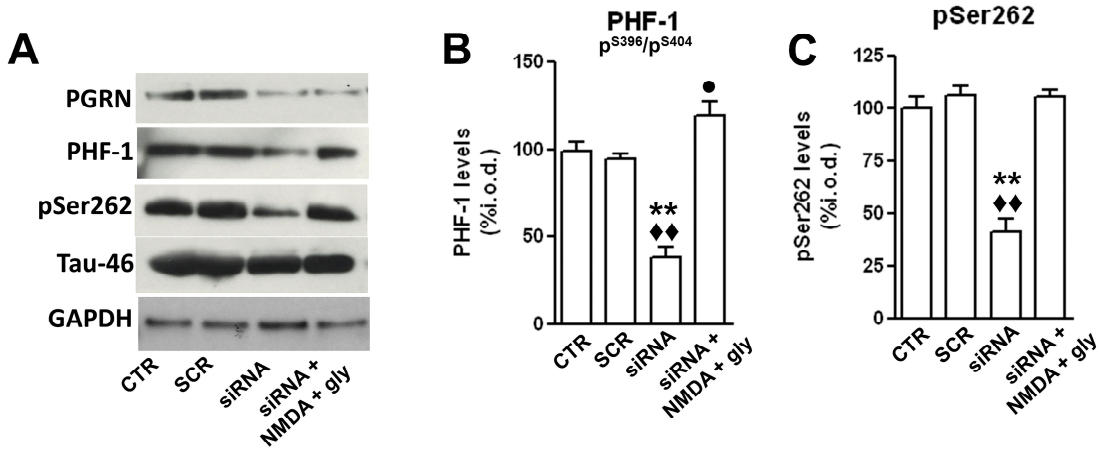

Figure 6